Materials Today Advances 18 (2023) 100363

Contents lists available at ScienceDirect

Materials Today Advances

journal homepage: www.journals.elsevier.com/materials-today-advances/

Deconstructed beetles: Bilayered composite materials produce green coloration with remarkably high near-infrared reflectance

Laura Ospina-Rozo [a, *], Niken Priscilla [b], James A. Hutchison [c], Allison van de Meene [a], Nicholas W. Roberts [d], Devi Stuart-Fox [a], Ann Roberts [b]

[a] School of Biosciences, University of Melbourne, Parkville, Victoria, 3010, Australia
[b] ARC Centre of Excellence for Transformative Meta-Optical Systems, School of Physics, University of Melbourne, Parkville, Victoria, 3010, Australia
[c] ARC Centre of Excellence in Exciton Science, School of Chemistry, University of Melbourne, Parkville, Victoria, 3010, Australia
[d] School of Biological Sciences, University of Bristol, Bristol Life Sciences Building, 24 Tyndall Avenue, Bristol, BS8 1TQ, UK

ARTICLE INFO

Article history:
Received 24 June 2022
Received in revised form
26 October 2022
Accepted 26 March 2023
Available online 3 April 2023

Keywords:
Scarabeidae
Near-infrared
Light manipulation
Cooling coatings
Photonic crystals
Broadband

ABSTRACT

Beetle elytra (hardened forewings) are a promising source of inspiration to develop or enhance the performance of human-fabricated composite materials. The structures responsible for optical properties in the ultra-violet to visible spectrum (300–700 nm) have been extensively characterised, but we have limited knowledge of optical properties and their physical origin in the near-infrared (NIR; 700–1700 nm). We examined the elytra of three species of green scarab beetles (*Xylonichus eucalypti*, *Anoplognathus prasinus* and *Paraschizognathus olivaceus*) with very high NIR reflectance. We manually separated layers in the elytra to disambiguate their contributions to the overall optical response. We show that unlike other scarabs, nanostructures within the cuticle layer do not produce notable reflectance. Instead, the cuticle resembles a pigment-based filter with 50% transmittance in the NIR and absorption in the visible spectrum contributing to the green appearance. Each species has a layer below the cuticle that appears white to the naked eye and produces broadband reflectance, particularly in the near-infrared; however, the structure of the white underlay differs markedly between the three species. In *A. prasinus* and *P. olivaceus*, the structure is disordered (no regular, repeated elements at optical length scales); whereas in *Xylonichus eucalypti*, the white underlay was notably thinner and comprised quasi-ordered hollow cylindrical structures embedded in a chitin matrix. We modelled the coherent scattering produced by this structure to demonstrate that it is responsible for broadband visible and NIR reflectance. We discuss biological implications and technological applications of the composite structure of beetle elytra.

1. Introduction

Composite materials combining different structural and functional properties are ubiquitous in nature and of substantial interest in materials science [1]. The mechanical properties of natural composite materials have been the subject of substantial interest [2], but the contributions of different layers to optical responses in different wavebands have received little attention. Most photonics studies have focused on structures that manipulate UV–visible light (UV-VIS: 300–700 nm) in natural materials such as butterfly wings, insect cuticles and bird feathers [3–6], but very few have examined structures contributing to near infrared (NIR: 700–2500 nm) optical responses [chameleons: [7,8], birds: [9]]. This is important for passive cooling (i.e. reducing absorption of radiative heat) because NIR wavelengths account for approximately half of the radiant energy in direct sunlight [10]. Understanding the properties and architecture of the natural structures that interact with NIR light is important to understand the biological relevance of NIR reflectance and its potential for bioinspired applications.

In both animals and manufactured materials, passive cooling can be effectively achieved by using bilayer composite materials that reflect light differently in visible and NIR wavebands. For animals, visible colour is important for camouflage or signalling;

* Corresponding author.
E-mail addresses: laura.ospinarozo@unimelb.edu.au (L. Ospina-Rozo), npriscilla@student.unimelb.edu.au (N. Priscilla), james.hutchison@unimelb.edu.au (J.A. Hutchison), allison.van@unimelb.edu.au (A. van de Meene), Nicholas.Roberts@bristol.ac.uk (N.W. Roberts), d.stuart-fox@unimelb.edu.au (D. Stuart-Fox), ann.roberts@unimelb.edu.au (A. Roberts).

https://doi.org/10.1016/j.mtadv.2023.100363

while reflection of NIR light, which is largely invisible to most species, can aid thermoregulation [10]. Similarly, passive radiative cooling is increasingly important to mitigate the temperature rise in transformed environments and reduce the costs and environmental impact of energy powered cooling systems [11–14]. The traditional solution has been to chemically modify substances to increase their NIR reflectivity, however these chemicals are toxic or involve toxic components in their synthesis and they can also deteriorate over time [15]. More recently, bilayer coatings have been developed to provide a more effective alternative. These bilayer coatings comprise a broadband reflective underlay to maximise scattering of NIR light and reduce solar heat gain; and an upper layer to filter some of the reflected wavelengths in the visible spectrum to produce the desired colour. This has been proposed as a scalable and effective solution to facilitate the cooling of buildings [11–14], which is more effective and environmentally friendly than NIR reflective chemically altered pigments [15,16].

Beetles are a promising source of inspiration to develop or enhance the performance of human-fabricated composite materials for passive cooling. Beetles are the most diverse and successful animal group on earth and a major focus of bioinspired materials design [1]. Key to the success of beetles in colonizing almost every environment on earth is the modification of the first pair of wings into a shield covering the body – the elytra [17,18]. Beetle elytra are a natural composite material with different layers and air sacs to be able to simultaneously serve multiple functions, for example: light weight for flight, protection from mechanical damage (both strain and impact), hydrophobicity, self-assembly and many others [19]. Thus, beetle elytra comprise modular and multipurpose structures

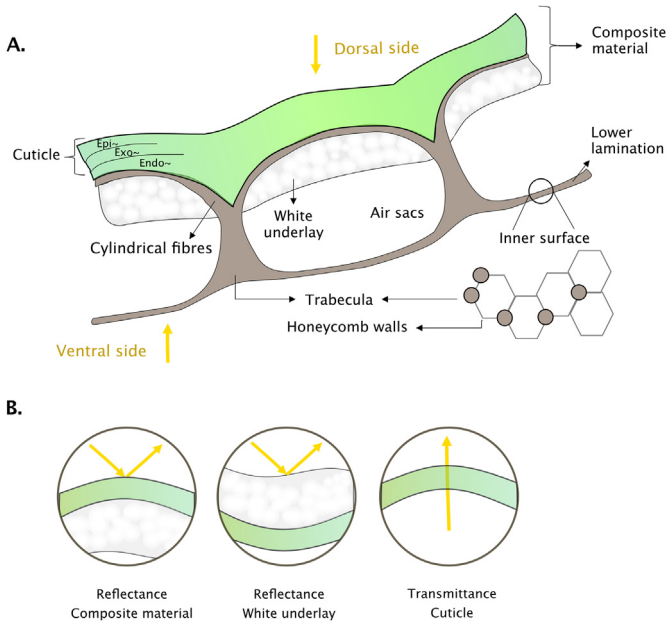

Fig. 1. Schematic of the composite material of beetle elytra. A. In the studied beetle species, a white underlay is located immediately under the upper lamination, and these two elements constitute the composite material. The upper lamination is composed mainly by the cuticle which can be subdivided in epicuticle, exocuticle and endocuticle. The air sacs between laminations ensure the elytra are sufficiently light weight for flight [25]. The ensemble of the honeycomb walls and trabecula confers mechanical stability to the elytra [22]. **B.** Examples of different configurations used to measure the optical properties of the two layers forming the composite material. Measuring reflectance from the dorsal side can be used to study the optical properties of the whole elytra or the intact composite (after removing the lower lamination). Measuring reflectance from the ventral side can be used to study the properties of the white underlay. Transmittance can be measured dorsally or ventrally. To study only the cuticle, we manually removed the white underlay.

to simultaneously accommodate multiple functions. The general architecture of beetle elytra is a sandwich structure (Fig. 1A). The upper lamination (outermost dorsal surface) and lower lamination (ventral side of the elytra: surface facing the body of the beetle) are separated by a series of air sacs and trachea. The inner surface of the lower lamination contains a honey-comb array of walls. In the intersections of these walls vertical cylinders called trabeculae connect the upper and lower lamination [20–22]. The upper lamination is mainly constituted by the cuticle, which has been the main focus of research because it contains diverse nanostructures that give rise to dazzling optical effects such as metallic, mirror-like and iridescent appearance [23]. These effects may be produced by one or more layers of the cuticle, known as epicuticle, exocuticle, and endocuticle [23]. Traditionally, it has been considered that the main role of the trachea, trabecula, fibres of the trabecula and the honeycomb structure is to provide structural support [2,19,21,22,24]. Thus, their contribution to the overall appearance of the elytra and NIR optical response remains unknown.

Optical effects from the beetle elytra are generally attributed to coherent scattering by very regular nanostructures, but given the diversity of beetle species, some species may have structures and mechanisms that remain unexplored. For example, beetles of the scarab family (Scarabidae) commonly have chitin fibres arranged in a helicoidal chiral structure (also known as Bouligand or plywood array) with optics analogous to a cholesteric liquid crystal (Fig. S2.) [26,27]. This helicoidal structure results in circular birefringence which produces optical activity [28]; and mechanical fracture resistance [29]. These Bouligand structures are widespread in nature and are of significant interest to materials scientists [30–32]; however, polarization (as a proxy for the presence of the chiral structures) is present in only 8 out of 15 subfamilies of Scarabeidae [33]. Thus, it is possible that other scarabs have alternative mechanisms to manipulate light. Furthermore, in contrast to optical responses in the visible spectrum, the nanostructural architecture underlying the high diversity of NIR light manipulation in scarabs [34] remains a mystery. From previous observations in Christmas beetles, we noticed that some species of scarabs have a distinctive pale colour on the ventral side of the elytra, which can be seen with the unaided eye as a white underlay located in between the two laminations of the elytra (Fig. S1). We hypothesised that this layer could contribute to light scattering, particularly in the NIR.

We examined the elytra of three different beetle species from different genera of Scarabeidae family: *Xylonichus eucalypti*, *Anoplognathus prasinus* and *Paraschizognathus olivaceus,* which have a white underlay (Fig. 1A and S1) and produce a green appearance and high NIR reflectance from the dorsal side. We described the composition of the elytra in the three species and evaluated the contributions of the cuticle and white underlay to the overall appearance of the elytra. Our results suggest that unlike other scarabs, the three species studied here have a cuticle that is largely transmissive and does not reflect light with nanostructures. Instead, the elytra comprise composite materials with the upper cuticle layer acting as a green filter overlying a layer that produces broadband reflectance, which is higher in the near-infrared. Structural analysis of the white underlay revealed quasi-ordered structures (i.e. partial absence of organisation in either spacing, size or spatial disposition [35–37]) in *Xylonichus eucalypti*, in contrast to structures that were highly disordered at different length scales in the other two species. As only the structure of the white underlay of *Xylonichus eucalypti* was amenable to optical modelling, we modelled the coherent scattering produced by the quasi-ordered structures in this species to examine whether they are responsible for broadband visible and NIR reflectance. We discuss how the optical responses of composite materials in beetle elytra may be an advantage in different biological contexts as well

as a source of inspiration for passive cooling technologies.

2. Methods

2.1. Beetle elytra

The specimens of *Xylonichus eucalypti*, *Anoplognathus prasinus* and *Paraschizognathus olivaceus* were obtained from the Australian National Insect Collection (ANIC). We removed the left elytron of each beetle to conduct destructive sampling. The three species studied here have a white underlay located in between the two laminations (Fig. 1A and S1). We use the term white underlay as a proxy descriptor based on the visual appearance, since the origin of this material may be different for the three species. This white underlay together with the upper lamination form the composite material of interest (Fig. 1A). To study the composite material, we carefully removed the lower lamination of the elytra with a scalpel. Since the major component of the upper lamination is the cuticle, we use this term for brevity. We contrasted the properties and structure of the composite material with those of the cuticle with the white underlay removed. It is not possible to examine the white underlay in isolation because it cannot be removed from the cuticle without damaging it (Fig. 1B).

2.2. Spectral measurements

To measure the macroscopic sample reflectance (spot size 4 mm diameter), we obtained hemispherical reflectance spectra of the beetle elytra while still attached to the beetle body with an integrating sphere containing an inbuilt tungsten-halogen light source (400−2100 nm; ISP-REF; Ocean Optics Inc., Dunedin, FL, USA.) and 4 mm diameter sampling port connected to two spectrophotometers (Ocean Optics Inc., Dunedin, FL, USA), a USB 2000+ (400−1000 nm) and NIRQuest (1000−2100 nm) via a bifurcated optic fibre. Measurements were recorded using the software OceanView 1.6.7. and calibrated against a diffuse 99% reflectance spectralon standard (Labsphere, North Sutton, NH, USA).

To measure transmittance/direct transmission [38] we used a standard set up in which the spectrometers and light source are carefully aligned to send a beam of light through the sample and collect, on the opposite side, the portion of the beam that was neither absorbed nor scattered. For each measurement we placed one elytron between the light source and spectrometers. We used two light sources to include the UV−Visible range (PX-2 pulsed Xenon light) and the visible-NIR range (HL-2000 tungsten halogen light), combined via bifurcated optical fibres to illuminate the sample from the dorsal and ventral side of the elytra. To prevent saturation, we placed an 80% filter (SMA-ADP-031; Ocean Insight, USA) and a 0.4 neutral density filter (ND204B; Thorlabs Inc., USA) after the HL-2000 tungsten halogen light. We used the same two spectrometers connected to a bifurcated optic fibre to capture the light on the other side of the sample. Measurements were recorded with the same software and calibrated against the reference (parallel beam of light without the sample).

To obtain macroscopic reflectance measurements of the different layers of the composite material (Fig. 1B), we used the same spectrometers and light sources coupled to a goniometer. This allowed us to fix both the angle of incidence and collection to 15° from the normal [39] and reduce the sampling area to a 1-mm diameter spot to focus on the areas of the elytra that were manually altered. We calibrated measurements against a diffuse 99% reflectance spectralon standard (Labsphere, North Sutton, NH, USA). As measurements were taken at the specular angle, it is possible to obtain values > 100% reflectance relative to the diffuse standard but these values are not problematic since all samples were compared to the same reference [39]; however the samples were primarily diffuse, so measurements of reflectance at the specular angle are a reasonable descriptor of the reflectance integrated across angles [39].

We measured the reflectance of the intact elytra (i.e. with the lower lamination), the white underlay (i.e. the composite material, measured from the ventral side) and the cuticle (i.e.; underlay removed; Fig. 1B). We measured transmittance of the composite material (elytra without the lower lamination) and the cuticle. It is not possible to measure transmittance of the white underlay since it cannot be isolated from the other components without damaging it. The transmittance and reflectance profiles were analysed with the R package pavo [40].

2.3. SEM microscopy

We used high resolution scanning electron microscopy (SEM) to explore the composition of the beetle elytra and to identify the structures that comprise the white underlay in the three species by comparing elytra with and without the white underlay. We used a sharp blade to cut transversal sections (perpendicular to the antero-posterior axis of the beetle) from the intact elytra and the cuticle (after removing the lower lamination and the white underlay) of the three species under a dissecting light microscope. Subsequently, the samples were mounted on independent stubs with carbon conductive tape and then sputter-coated with gold for 3 min using a QT5000 sputter coater (Quorum, United Kingdom). Finally, the samples were analysed using a SU7000 field emission scanning electron microscope (Hitachi, Japan) at 2.00 kV. In order to determine whether the quasi-ordered nanostructures in the white underlay of *X. eucalypti* consisted of a series of spherical air bubbles or air cylinders, we repeated the same procedure with longitudinal sections of the elytra (parallel to the antero-posterior axis of the beetle). Finally, in order to extract the dimensions of different parts of the elytra, we analysed the SEM images of the three studied species with the basic measuring tools in Fiji, ImageJ [41].

2.4. Microscatterometry

We used microscatterometry to obtain angle-resolved spectral measurements of components of the composite materials of beetle elytra at the microscopic scale. The microscatterometry measurements were limited to the visible spectrum due to the wavelength limits of silicon-based technologies that form the basis of all optical microscopy. The set up consists of a highly focused broad band tungsten-halogen light source (Ocean Optics HL-2000) coupled to a microscope objective (Olympus, oil immersion (Leica, refractive index 1.518×), 60× magnification, numerical aperture 1.42). The broad band source was collimated and expanded to fill the objective back aperture, thus illuminating the sample at angles from 0 to 69° from the surface with a focal spot of approximately ~1 μm diameter. The light scattered by the sample was recovered by the same objective and an image of the objective back focal plane was projected onto a CCD camera (PIXIS 1024B, Princeton Instruments) via a spectrograph (Acton SP2300, 150 grooves/ml grating), see Schematic in Fig. S3. In this way, microscopic reflection spectra could be collected over an angle range from 0 to 69° from the surface normal in a single shot (see Fig. 5). Reflectance was measured with respect to an aluminium film reference. This technique has been used effectively to study light manipulation by structures in biological samples [42], and we used it here to explore the optical properties of each component of the composite material across multiples angles of incidence and reflectance. To study the intact composite material, we measured its reflectance dorsally. To

study the white underlay, we measured the reflectance of the composite material ventrally. We selectively focused the illumination plane of the microscope objective on the white underlay ignoring the cuticle, since it is impossible to separate the white underlay from the cuticle without damaging it. Finally, to study the cuticle, we carefully removed the white underlay and measured the cuticle's reflectance and transmittance (Fig. 1B). Transmittance measurements were calibrated against the illumination beam of the microscope in the 60x objective (as described above) without any sample on the stage. All samples were mounted on glass coverslips (170 μm thick) and immersed in objective immersion oil (Leica, refractive index 1.518) for refractive index matching to the coverslip/objective couple.

2.5. TEM microscopy

Our measurements of the optical properties of the layers in the composite material showed that the white underlay in *Xylonichus eucalypti* is the most NIR reflective of the three studied species. Additionally, the SEM images showed that the white underlay of *A. prasinus* and *P. olivaceus* comprised structures that are highly disordered at different length scales; whereas in *X. eucalypti*, the white underlay is much thinner in cross-section and comprises a quasi-ordered structure that may produce coherent scattering. To characterise these structures so that we could model the coherent scattering, we used transmission electron microscopy (TEM) to reconstruct a 3D model of *X. eucalypti* from transversal sections and to characterise the shape, spacing and orientation of the nanostructures. We did not perform TEM for *A. prasinus* and *P. olivaceus* due to the length scale of the structures in the underlay and because the structures are not amenable to analytical modelling. For TEM of *X. eucalypti*, we followed the standard procedure for block face imaging: we stained the samples with heavy metals, dehydrated them in subsequent dilutions of ethanol and acetone, and embedded them in Spurr's resin (ProSciTech) [43,44]. We obtained serial sections of 70 nm thickness up until completing the sectioning of 1 μm depth in the sample, with an EM UC7 ultramicrotome (Leica, Germany) and imaged them using a Tecnai™ Spirit transmission electron microscope (FEI – ThermoFisher, United States).

In order to determine the shape, orientation and separation of the particles in the white underlay of *X. eucalypti*, we sampled 5 rectangular regions of 6 × 4 μm of the white underlay from each of the TEM images. We transformed the TEM rectangles into a binary image showing dark electron-dense regions that represent the chitin matrix and white patches that represent the air space inside the cylinders. Then, we used the plug-in 'Analyze particles' in Fiji, ImageJ [41] to automatically identify these white patches, also called regions of interest (ROI), number them and fit an ellipse to each of them. From this plug-in we obtained the following parameters for 738 ROI: x and y centroid (indicating the position of the ROI in the image), major and minor axis of the correspondent ellipse, aspect ratio (ratio between the major and minor axis), circularity (proportion between the area and perimeter of the ellipse) and angle between the primary axis and a line parallel to the x-axis of the image (indicating if the ellipses have a random orientation in the matrix). In addition, for 88 ROI we identified an adjacent ROI and calculated the centre-to-centre distance by calculating the Euclidean distance between their centroids. All statistical analyses were carried out in the software R [45]. Finally, to produce a 3D reconstruction of the structures in the white underlay of *X. eucalypti*, we aligned the consecutive transversal TEM sections and selected features that consistently repeated across images. These features were followed through the sections and assembled together using the software Midas – IMOD [43,44,46].

2.6. Computational modelling

We implemented computational models to investigate the physical origin of the optical response of the quasi-ordered structures in the highly NIR-reflective white underlay of *X. eucalypti*. We created a 2D photonic crystal model assuming the structure to be a chitin matrix with air cylinders aligned along the longitudinal axis of the elytron (here equivalent to the z plane) (Fig. S4.). We implemented a 2D photonic crystal model because our SEM longitudinal images showed that the structures in the white underlay had a more cylindrical rather than spherical geometry (Fig. 6A). We analysed the interaction of the structure with light of different wavelengths and polarizations using the Finite Element Method (FEM) as implemented in COMSOL Multiphysics (5.6)® [47]. We modelled the underlay as a hexagonal array of identical cylindrical air voids (refractive index, $n = 1$) with circular cross-sections embedded in a chitinous matrix (refractive index of $n = 1.5$). The wavelength-dependence of the index of refraction of chitin is well known [48,49], however we used a refractive index of 1.5 because this value is a good approximation to describe the interactions with visible and near-infrared light, and we did not consider UV wavelengths in our models [49]. The array was assumed infinite in the transverse x-direction and included 5 rows of cylinders in the vertical y-direction. Periodic boundary conditions were applied on the sides, non-reflecting ports implemented on the excitation and output boundaries, and the wavelength was swept from 400 nm to 1700 nm. Plane waves were incident on the structure from the y axis and both z-polarization (electric field parallel to the axis of the cylinder, i.e. the antero-posterior axis of the elytra) and x-polarization (electric field perpendicular) excitation was considered. The output of these models are the simulated reflectance spectra. Since no absorption was assumed in the model, the transmission was given by the inverse of the reflectance.

We considered different scenarios based on the parameters obtained from analysis of TEM images. To examine the effect of the particle size we created three models assuming circular cylinders with a right section (transversal) of 602, 660 and 732 nm diameter and constant centre-to-centre distance of 868 nm. Given that the right section of the cylinders in the white underlay was fitted to an ellipse (not a perfect circle) in our image analysis, we determined the diameter of the cylinders in our models as the average of the minor and major axis of the ellipses at the 25, 50 and 75% percentiles respectively in our measurements from TEM images (Table 2). To examine the effect of particle separation, we created two models assuming circles with 660 nm diameter and centre-to-centre distance of 732, 868 and 967 nm corresponding to the 25, 50 and 75% percentiles respectively in our TEM measurements (Table 2). To evaluate if the structure had polarization sensitivity, we compared the two polarizations x and z in all these models. Finally, to test the effect of different angles of incidence we compared two models with cylinders of 660 nm diameter at 868 nm centre-to-centre distance, and incident light coming from the normal or 30° angle. Overall, this set of models enabled us to explore whether the structures in the white underlay of *X. eucalypti* produce coherent interference but incorporate enough variability to produce diffuse reflectance of visible and NIR light (consistent with our spectrometry data) instead of directional, specular and/or iridescent reflectance.

Finally, considering that the white underlay in *X. eucalypti* seems to contain a considerable degree of disorder, we also ran numerical

simulations of the structure using a custom MATLAB script adapted from the algorithm previously used to study quasi-coherent scattering from similar structures with two distinctive refractive indices producing diffuse blue scattering in birds [35,36] (Supplementary materials S8).

We did not model the white underlay of the remaining two species *A. prasinus* and *P. olivaceous* because the structures are not amenable to straightforward analytical modelling. Some disordered arrays such as the ones in the ultra-white scales of some beetles have been modelled as disordered multilayers, since a transversal section of the array reveals intercalating layers of tissue and air [50–53]. This approach is not appropriate for *A. prasinus* and *P. olivaceous* because the sheets and air cavities in the structures are greater than the relevant optical length scales (¼ λ as expected for multilayers [38]). Similarly, although Mie scattering can predict the reflectance of disordered arrays [37], the chitin sheets in the white underlay are flat and folded instead of spherical, and no exact solutions can be obtained using the T-matrix method for non-spherical scatterers [37]. This is an interesting problem and will be the subject of ongoing work.

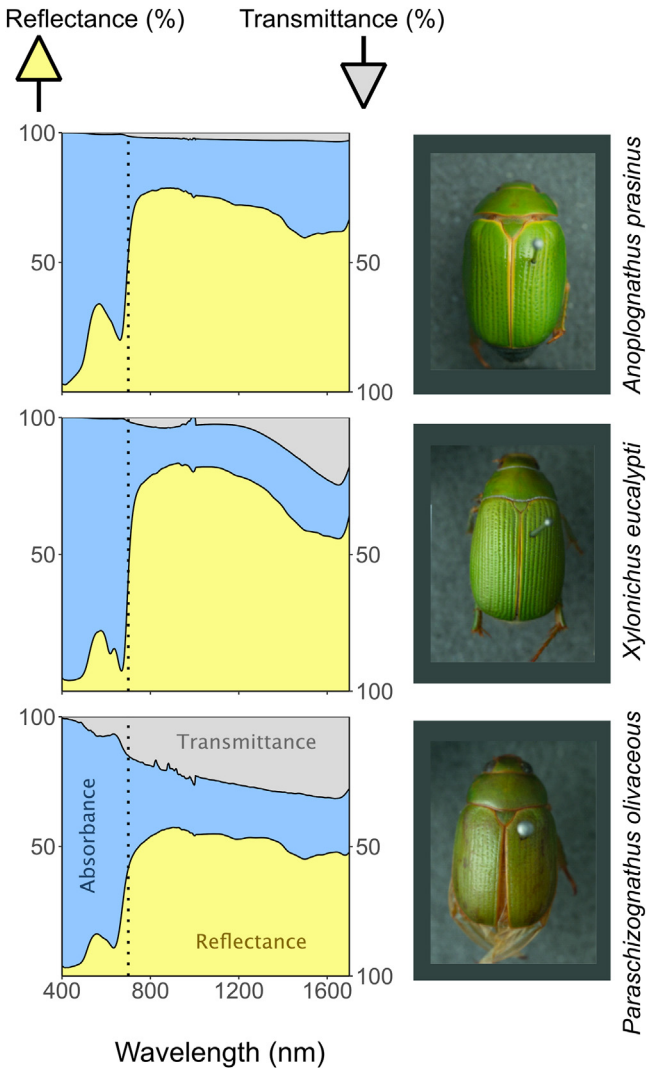

Fig. 2. Optical properties of the elytra of three beetle species. Spot size = 4 mm. For each species we show the reflectance and transmittance profile with regular and inverted y-axis respectively. The area in the middle represents the amount of light absorbed by the elytra.

3. Results

3.1. Optical properties on the macroscopic scale

The three beetle species had similar reflectance profiles corresponding to green appearance and high NIR reflectance but different transmittance profiles (Fig. 2). *P. olivaceus* had the lowest reflectance and highest transmittance, while *A. prasinus* had the highest reflectance and lowest transmittance (<10%). Considering that the proportion of light that is neither reflected nor transmitted is equivalent to the light absorbed by the material [38], we also determined that the elytra of *A. prasinus* had the highest absorbance (Fig. 2).

3.2. Architecture of the composite materials

Our SEM imaging allowed us to precisely identify the parts of the elytron that comprised the white underlay. In *A. prasinus* and *P. olivaceus* this structure was in the air sacs of the elytra. In *X. eucalypti* it was located underneath the fibres commonly associated with the endocuticle and the epidermal cells, while the air sacs remained empty (Fig. 3). In *A. prasinus* the white underlay was composed of a disordered cavernous structure formed by tightly packed chitin sheets that fold in a disordered manner creating microscopic cavities of air. For this species, the white underlay extended all the way between the upper and lower laminations filling the space that is usually empty for most scarab species. Tracheae appear embedded inside the white underlay (left panel in Fig. 3). In *P. olivaceous* the white underlay also was formed by chitin sheets, but they were less packed and less folded. Instead, most of them were perpendicular to the laminations with opposite ends of the sheets often attaching to the upper and lower laminations. In both *A. prasinus* and *P. olivaceous* the sheets of the white underlay were highly corrugated (right panel in Fig. 3). In *X. eucalypti*, the white underlay was notably thinner and did not contain corrugated sheets. Instead, it comprised hollow cylindrical structures embedded in a chitin matrix. The cylinders appear as an array of nanoscopic circles in a transversal SEM section (Fig. 3 central panel) and as long grooves in a longitudinal SEM section (Fig. 6A). Although these cylinders were not perfectly aligned, they can be considered a quasi-ordered structure since they are relatively similar in size and spacing.

Overall, the SEM data showed that the cuticle is similar for the three species (Fig. 3 bottom panel), but the structures of the white underlay differ greatly and have different degrees of disorder. The dimensions of the elytra and its subdivisions also differ for these three beetles (details in Table 1.). In addition, these results highlight that our manual protocols to deconstruct the beetle elytra into its constitutive elements was effective, which was crucial for our interpretation of the measurements of optical properties in different configurations (as shown in Fig. 1B and further explained below).

3.3. Optical properties of the different elements in the composite materials

In all three species, the cuticle had very low reflectance across the spectrum in comparison to the white underlay (Fig. 4). We did not, in fact, obtain significant reflectance from the cuticle alone with microscatterometry. Additionally, the cuticle was transmissive in longer wavelengths >700 nm (~50% of the light Fig. 4), while it transmitted only a maximum of ~30% in wavelengths <700 nm (Fig. 4) with minima around 650 nm (Figs. 4 and 5). These minima are accentuated in the reflectance profile of the whole elytra (in comparison to the cuticle alone, Fig. 4). Considering the low

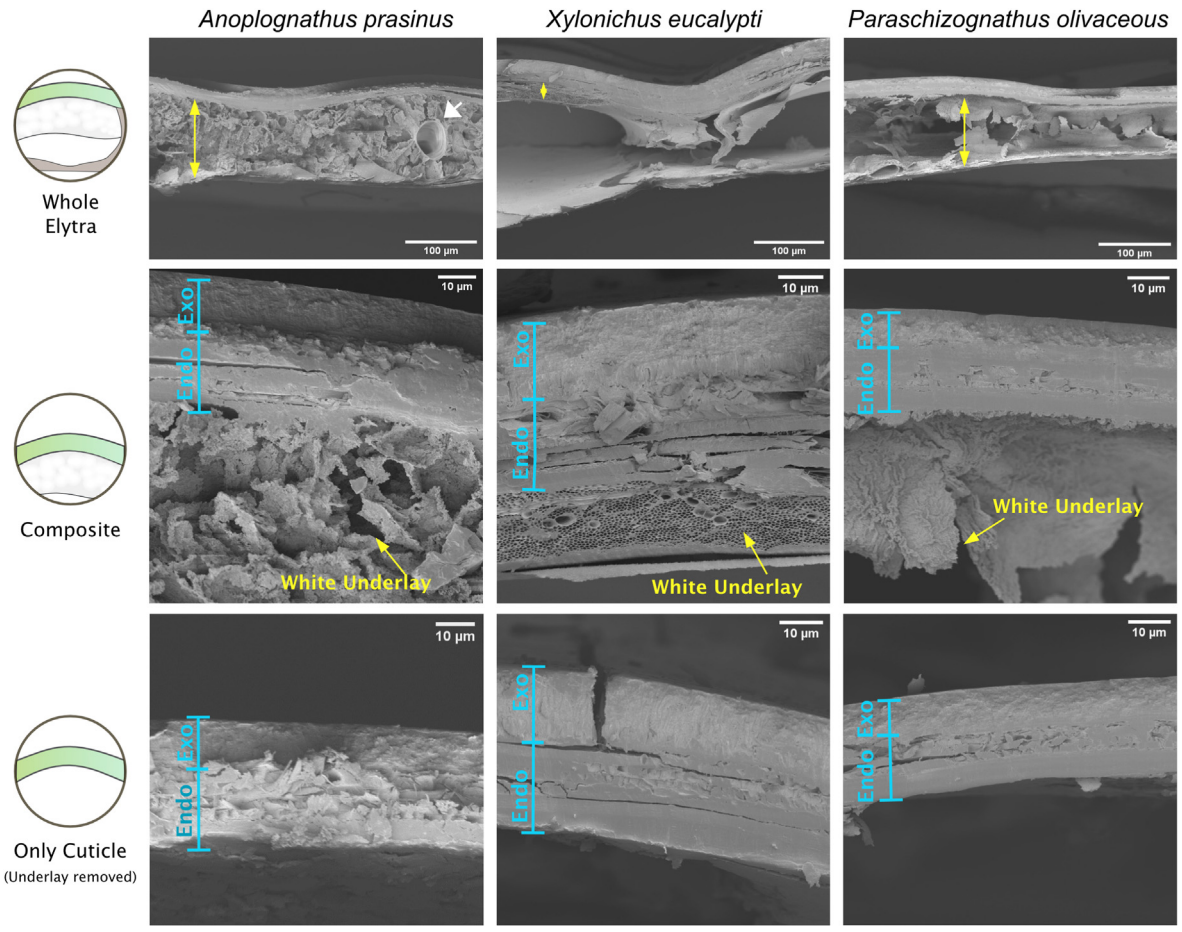

Fig. 3. Architecture of the composite materials. Top row: SEM images of transversal sections of the elytra. Upper and lower laminations are visible as well as the air sacs in *X. eucalypti* and *P. olivaceous*, and the trachea in *A. prasinus* (white arrowhead). Vertical double-headed arrows highlight the differences in thickness of the white underlay for these three species. Middle row: Two subdivisions of the cuticle are shown: exo and endocuticle. The epicuticle is located dorsally to the exocuticle, but it is indistinguishable at this magnification. The structures of the material below the endocuticle are very different for these three species. Bottom row: the cuticle after manually removing the white underlay.

Table 1
Dimensions of different parts of the elytra in the three species. All measurements are given in µm and in the format mean ± sd, considering measurements of three different SEM images per species. Images processed in FIJI ImageJ.

	A. prasinus	X. eucalypti	P. olivaceous
Elytra – Max. thickness	157.10 ± 1.51	218.65 ± 9.14	140.25 ± 8.09
Elytra – Min. thickness	134.67 ± 0.02	145.53 ± 0.56	95.64 ± 4.59
Air sacs - Av. thickness	closed	156.38 ± 25.56	86.26 ± 19.11
Trachea–- Diameter	47.54 ± 7.86	Not seen	Not seen
Upper lamination–- Thickness	33.72 ± 1.42	57.71 ± 1.19	22.82 ± 0.87
Exocuticle - Thickness	11.86 ± 0.33	14.43 ± 2.57	9.85 ± 1.32

reflectivity of the cuticle, the transmittance minima are likely due to absorption attributed to the presence of pigment and consequently could be associated with the green appearance of these beetles. The *Xylonicus eucalypti* cuticle had one additional high energy minimum which could be due to a pigment absorption vibrational replica or the existence of a different pigment (Fig. 5).

In contrast to the transmissive cuticle, the white underlay of all three species had high broadband reflectance, which was notably higher in the NIR (>700 nm) than in the visible spectrum (Fig. 4). The white underlay also reflected light diffusely across a wide range of angles (up until 900 nm in Fig. 5) as expected for these species [34]. The reflectance spectra of the white underlay in *A. prasinus* and *P. olivaceous* are similar with increasing reflectance in the longer visible wavelengths and a homogeneous flat reflectance beyond 900 nm around 40%, while the reflectance spectra of *X. eucalypti* had two broad maxima (peaks) with reflectance higher than the other two species across the full spectrum (>100%, i.e., even greater than the Lambertian surface of the white standard) (Fig. 4). The microscatterometry results also showed that the white underlay of *X. eucalypti* was the most reflective of the three species in the visible range (Fig. 5). The reflectance of *P. olivaceous* appeared to be much weaker when measured with microscatterometry (Fig. 5) than with spectrometry (Fig. 4). The elytra (with the lower lamination) seem more reflective than the white underlay for *A. prasinus* and *P. olivaceous* in the spectral data (Fig. 4) but not in the microscatterometry data (Fig. 5). This could be because for these two species, the white underlay may suffer small alterations after the removal of the lower lamination potentially causing

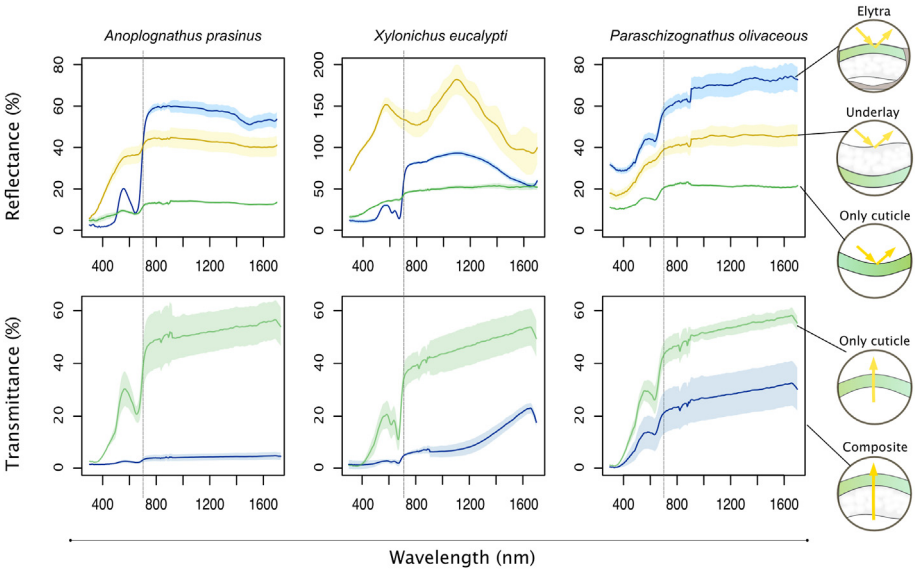

Fig. 4. Optical properties of the different elements in the composite material at the macro scale. Reflectance was measured at the specular angle. For the three species, the white underlay is a broadband visible and NIR reflector while the cuticle has lower reflectance accross the spectrum (gray vertical lines at 700 nm). *X. eucalypti* is the species with the most reflective white underlay (note the scale in the y axis). The reflectance on the dorsal side of the elytra differs from the reflectance of the white underlay. The cuticle is more transmissive than the intact composite (cuticle + white underlay).

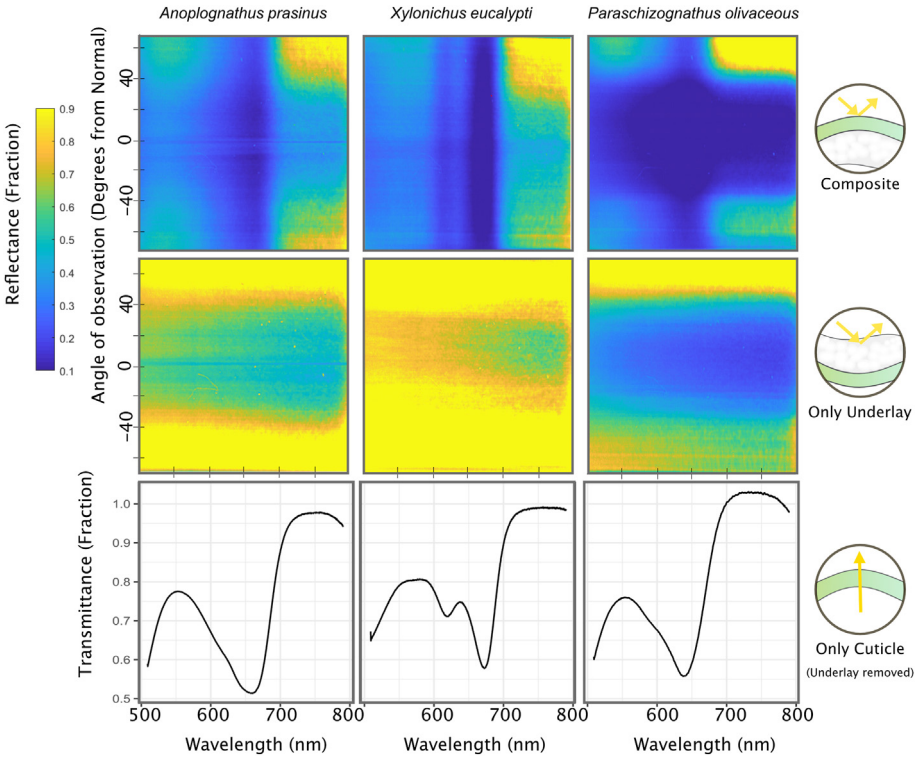

Fig. 5. Reflectance in multiple angles and transmittance. Scatterometry results. The samples were illuminated with unpolarized light, but the collected light was filtered for the x-polarization (electric field perpendicular to the plane of incidence of the light over the filter). For the three scarabs, the diffuse reflectance pattern as a function of angle produced by the composite material (top) is the result of the additive interaction between the underlay reflectance (middle) and cuticle transmittance (bottom), in other words between the structural and filtering component in the composite material. The transmittance spectra of the cuticle of the three beetles are remarkably similar.

underestimation of the white underlay reflectance apparent only at the macro level.

The composite material (cuticle + white underlay) measured form the ventral side (white underlay facing the light source) also varied in transmittance between species. Low transmittance of the composite in this configuration is expected for *X. eucalypti* (<10%) since most of the light is reflected by the white underlay, therefore it cannot be transmitted. Remarkably, the white underlay of *A. prasinus* and *P. olivaceous* have a similar reflectance, but the composite material in *P. olivaceous* has high transmittance

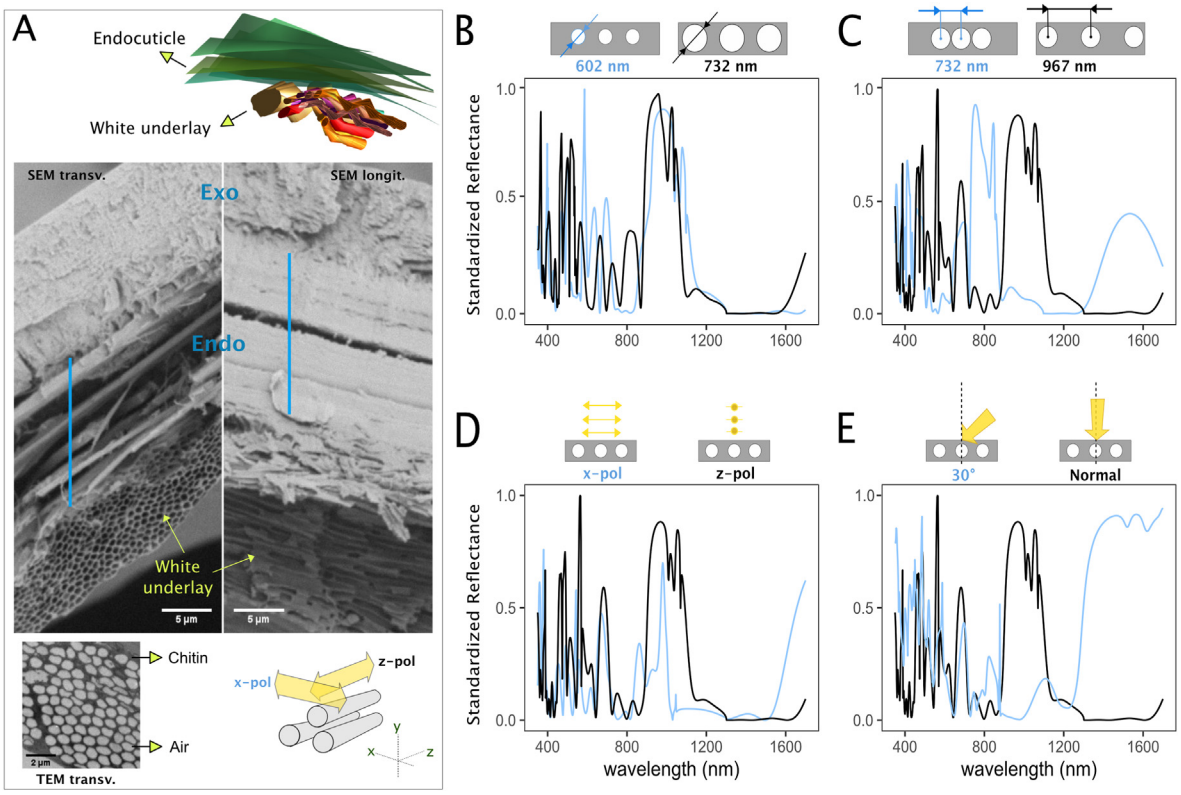

Fig. 6. Modelling of the white underlay of *X. eucalypti*. A. We produced a 3D reconstruction of the structures in the white underlay by following the white circles (air spaces in the chitin matrix) through subsequent transversal TEM sections. We confirmed that these circles correspond to the transversal section of cylinders with longitudinal SEM sections. Thus, we modelled the white underlay as cylinders interacting with light in two polarizations: with its electric field parallel to the cylinder axis (z-pol) and perpendicular to the cylinder axis (x-pol). **B.** Effect of the size of the cylinders: comparing particles with different diameters (constant 868 nm centre-to-centre distance, normal incidence, z-pol). **C.** Effect of the separation between the cylinders: comparing different centre-to-centre distances (fixed 660 nm diameter, normal incidence, z-pol). **D.** Effect of the polarization of the incoming light (660 nm diameter and 868 nm centre-to-centre distance). **E.** Effect of the angle of incidence of the incoming light (660 nm diameter and 868 nm centre-to-centre distance, z-pol). SEM images in A showed that the cylinders are not perfectly ordered (quasi-ordered), which suggests that the overall reflectance of the structure is the sum of variations of the scenarios in B to E.

(reaching approx. 30% in the NIR), while the composite material in *A. prasinus* has the lowest transmittance of the three species (<5% across the full spectrum). This could be explained by high absorption in the white underlay of *A. prasinus*.

The microscatterometry shows enhanced reflectance at high angles (>40° from the surface normal) for all species, an effect commonly associated with total internal reflection. In this phenomenon, the incident light beam is completely reflected with no attenuation because it travels from a medium of higher refractive index onto a medium of lower refractive index at an angle greater than or equal to the critical angle [38]. Given that the beetle elytron has microstructures able to repel water and other substances [54], it is likely that the refractive index-matching oil in which the samples are immersed does not fully infiltrate the space in between the two laminations of the elytra. Thus, the enhanced reflection at larger angles could be produced by the interfaces between chitin/immersion oil (refractive index = 1.5) and air pockets inside the white underlay (refractive index = 1) for which the critical angle is 41°. However, disordered structures in other beetles can favour enhanced reflectance at larger angles for other reasons [53]. The asymmetry in reflectance at positive and negative angles from the normal could be a product of irregularities in the sample. Both the white underlay and the surface of the elytra contained irregularities at different scales and directions (Fig. S5.). Even after ensuring the best focusing of the light beam, the target surface may not be flat, further contributing to the asymmetry in reflectance. We used polarized filters to collect the light with electric field perpendicular to the plane of incidence (s-polarization) and with electric field in the plane of incidence (p-polarization) for different alignments of the elytron. In Fig. 4, we show the light reflected by the structures only in one polarization since we did not observe any obvious polarization events. This suggests that disorder in the nanostructures is enough to cancel any such polarization effects, or else the polarization sensitivity of the structure is too subtle to be detected by our set up.

3.4. Structure of the white underlay in Xylonichus eucalypti

As the white underlay of *Xylonichus eucalypti* comprised quasi-ordered structures at optical length scales, which could produce coherent scattering, we conducted a more in-depth structural analysis using TEM to parameterise computational models. The TEM images revealed considerable variability in the size, separation and orientation of the cylinders (Table 2). From the TEM image processing we found that the right section (transversal section) of the cylinders in the white underlay of *X. eucalypti* consists of ellipses with a fairly regular perimeter (circularity). The major axis of the ellipses varied between 603 and 1027 nm and minor axis between 290 and 646 nm (5% and 95% percentiles). We did not find any correlation between the separation of the ellipses and their size, i.e. the centre to centre distance was neither correlated with the ellipses major axis (Pearson's correlation R = 0.062, p-value = 0.567, C.I. −0.151; 0.271), nor the minor axis (Pearson's correlation R = −0.12, p-value = 0.259, C.I. −0.326; 0.091). The

Table 2
Characterisation of the transversal section of the cylinders in *Xylonichus eucalypti*'s white underlay.

Parameter	Mean	sd	Percentiles		n
			25%	75%	
Ellipse major axis	807.4	168.62	741.25	883	738
Ellipse minor axis	510.87	109.37	462	581	738
Aspect ratio	1.63	0.46	1.34	1.8	738
Centre-Centre distance	867.69	200.47	732.28	966.54	88
Circularity	0.83	0.11	0.79	0.9	738
Angle	20.85	14.86	10.04	29.06	737

major axis of the ellipses roughly aligns with the surface of the cuticle and the ventral surface of the elytra but it varies between −30 and 30° (Fig. S6). The variability in the angles of the cylinders and in the thickness of the chitin matrix can explain the lack of correlation between the size of cylinders and their separation. From the 3D reconstruction we conducted based on sequential TEM images and the longitudinal SEM images (Fig. 5A) we also observed that the cylinders do not align perfectly parallel to each other's axis. Instead, they zigzag and bend slightly adding disorder to the structure.

3.5. Computational models

According to our models (Fig. 6B–E) the two factors explaining the broadband reflection and high NIR reflection in *X. eucalypti* are the high variability in spacing between cylinders and the response of the structure to incident light from different angles. A change from the 25% percentile to 75% percentile in the size of the cylinders causes only a subtle change in the total reflectance (Fig. 6B), while an equivalent change in the spacing of the cylinders causes a significant shift in the reflected wavelengths (Fig. 6C). Not surprisingly the modelled structure has different responses for the two polarizations (Fig. 6D). This result contrasts with our experimental measurements that showed no polarization sensitivity, which could be because the cylinders do not perfectly align along a common z axis as shown by our morphological analysis and 3D reconstruction (Fig. 6A). Finally, the incident angle has a considerable effect on reflectance (Fig. 6E). At larger angles away from the normal, more NIR light is reflected.

Our models are simplified scenarios that combine and overlap in the natural white underlay in *Xylonichus eucalypti*. For instance, we showed that the reflected wavelengths depend on the spacing between the cylinders. The spacing between the cylinders, in turn, varies independently from their size (Fig. S6C). Thus, the presence of cylinders with variable spacing could produce different reflectance peaks which on average determine the broadband reflectance associated with white appearance and high NIR reflectance (consistent with results in Figs. 4 and 5 for the white underlay). We showed that the modelled structure responded differently according to the angle of incidence of the light and polarizations. Although our models suggest a highly regular structure with parallel cylinders will have polarization sensitivity, our SEM images showed that the cylinders in the white underlay are not perfectly parallel to each other (Fig. 6A). Disorder and misalignments are common in natural structures, and they generally reduce angle and polarization-dependent reflectance [37,55], which explains why we did not observe polarization sensitivity in the scatterometry measurements. The overall broadband reflection with two apparent peaks generated by the white underlay (Fig. 4) is likely the average of different responses of the structure across different angles and polarizations (Fig. S7), and overall broadband reflection as observed in our microscatterometry and spectroscopy measurements (Figs. 2 and 3). In short, the photonic crystal model and morphological analysis explain the broadband diffuse reflectance and high NIR reflectance by the white underlay in *Xylonichus eucalypti*.

The quasi-ordered matrix model [36] does not explain the reflectance of short wavelengths of less than 1000 nm (visible range) (Fig. S8) because the algorithm does not consider the polarization parallel to the axis of the cylinders, here called z polarization. Thus, in materials with cylinders like the white underlay of *X. eucalypti*, the reflected spectrum predicted by the adaptation of Prum and Torres's (2003) model corresponds only to the x polarization, i.e. when the electric field is perpendicular to the axis of the cylinders.

4. Discussion

In this study we demonstrated that contrary to other scarabs [27], the characteristic green appearance and high NIR reflectance of *Xylonichus eucalypti*, *Anoplognathus prasinus* and *Paraschizognathus olivaceus* is not produced by nanostructures in their cuticle. Instead, they combine optical effects produced by different layers of the composite structure of the elytra to create the overall optical response in the visible and NIR spectrum. The composite material in the elytra of three species comprises the cuticle and a white underlay. The underlay generates broadband diffuse reflection particularly high in wavelengths >500 nm, while the cuticle resembles a conventional pigment-based filter in the visible spectrum (green appearance), with a strong absorption dip around 560 nm and 50% transmittance in the NIR. Incident light that is not absorbed by the cuticle is reflected by the white underlay and transmitted through the cuticle a second time. Thus, the combined effects of the white underlay and cuticle explain the overall green appearance with high NIR reflectance. Despite the broad similarities between species, they differed considerably in the optical properties and corresponding architecture and nanostructures of the white underlay. Most notably, in *Xylonichus eucalypti*, the white underlay had much higher reflectance, particularly in the NIR, and was also much thinner, comprising hollow cylindrical structures aligned parallel to the surface and embedded in a chitin matrix. Our optical models of this quasi-ordered structure support the conclusion that they are responsible for broadband scattering and very high NIR reflectance in this species. Variation in the spacing and orientation of the cylinders, together with integration over multiple angles of incidence, appear to be key to the broadband scattering. By contrast, in *A. prasinus* and *P. olivaceus*, the structure of the white underlay is disordered, comprising chitin sheets with different structural dimensions and degrees of packing and folding in the two species. Although the structures are not amenable to optical modelling, we can infer that they are responsible for the observed broadband scattering based on our disambiguation of the optical response of the layers of the composite material. Overall, our results suggest that the composite materials in these beetles have characteristics analogous to coloured bilayer coatings, but broadband VIS and NIR reflectance of the underlay is produced by different structures in the three species. Additionally, considering that these three beetles are not sister species, it is possible that the bilayered structures arose due to convergent evolution in response to similar selection pressures, rather than due to common ancestry.

The developmental origins of both the white underlay and the cuticle may provide insight into why optical structures in *A. prasinus*, *X. eucalypti* and *P. olivaceous* differ markedly from other closely related scarabs, which appear to lack the white underlay. For example, is notable that the white underlay is formed by structures other than the cuticle. Given that the irregularly folded sheets forming the white underlay of *P. olivaceous* and *A. prasinus* are in the space between the two laminations, they may come from

the honeycomb, trabeculae or even the trachea [25]. The white underlay in *X. eucalypti* is located in the region immediately below the endocuticle and not in the air sacs, so it may come from the cylindrical fibres of the trabecula. These components in the elytra have traditionally been associated only with mechanical support [22] but we have shown that they also determine the optical properties of the elytra in some scarab species. Moreover, the insect tracheae contain spiral folds with corrugated surface called taenidia that function as structural support to prevent them from collapsing inwards [56]. The taenidia contain proteins and chitin fibres but lack cuticulin, which gives them a white appearance [57]. Tracheae and tracheolae increase light reflectance in other insect structures such as the tracheal tapetum [58–60]. The origin of the cuticle is also important. In the leaf beetle *Gastrophysa viridula,* a thin outermost green layer (absorption between 530 and 550 nm) is retained from the larva in the imago (adult immediately after ecdysis) but soon replaced by nanostructures [61]. It could be interesting to explore if the composite materials of the elytra in the studied species retain elements form the larva. Studies examining the development of the elements in composite materials of various species as well as its frequency among scarabs, could be combined with ecological and phylogenetic data, to facilitate insight into its evolutionary origin and adaptive value.

The structural component of the composite material — the white underlay — strongly determines the differences in total transmittance, absorbance and reflectance of the whole elytra of the studied species. For example, densely packed disordered arrays such as the one in *A. prasinus* are effective at producing high broad band reflection [11,62] in beetles [51,63–65], birds feathers [9] and plant mesophyll [66]. Although we did not attempt to model the white underlay of *A. prasinus* and *P. olivaceous*, we hypothesize that the chitinous sheets reflect light due to the difference in refractive indices between the air and chitin (like in plants [67]). The folding of these sheets creates air cavities, and the ridges and wrinkles increase their surface and disorder producing multiple scattering events. This idea is supported by the fact that *A. prasinus*, with densely packed chitin sheets in its white underlay has higher broadband reflectance than *P. olivaceous.* In addition, each time light is reflected by a surface, a proportion of that light is absorbed (structural absorption) [68–70], which could also explain why the thick white underlay from *A. prasinus* has the lowest transmittance of the three species. According to our models the quasi-ordered array in *X. eucalypti* formed by air cylinders in a matrix of chitin produces high broadband reflectance by slightly varying the size, spacing and spatial alignment [71] of the cylinders in the chitin matrix. The reason for the lower transmittance in this species could be that most of the light is reflected, but it could also depend on the absorption coefficient (determined by the imaginary part of the refractive index [38]) of the chitin forming the array. Understanding how beetles can achieve different combinations of transmittance, reflectance and absorbance in their elytra is key to investigate their biological role.

The structural component of the composite material determines the wavelengths reflected and the absence of angle dependent effects. For example, our results showed that the cylinders in the white underlay of *X. eucalypti* can be modelled as an array of photonic crystals with enough variation in spacing and orientation to produce broad band diffuse reflectance [52]. Unlike the highly ordered and aligned Bouligand structures present in other scarabs, this mechanism does not produce saturated peaks, iridescent reflectance, specular effects or circular polarization. Instead, the disorder in the structure results in enhanced white reflection as observed in other natural structures [72,73]. Worthy of consideration is the correlation between NIR and VIS reflectance. Due to the strong wavelength dependence of scattering [38], the nanostructures able to reflect NIR are likely to be relatively large and to interact with long wavelengths in the visible spectrum (red) and NIR. However, this is true considering only inter-scatterer correlations, i.e., the disposition of the particles in an array. If instead, the scattering behaviour of individual particles is also considered, secondary peaks of short wavelengths arise simultaneously [74]. This phenomenon combined with variability in the structures could produce multiple peaks in the NIR and VIS spectrum, which in turn explains why structures that reflect NIR tend to also be white [9] limiting the possibility of producing independent optical effects in the VIS and NIR wavebands with the same structure but increasing diffuse total reflectance.

The component of the composite material analogous to a pigment-based filter has similar optical properties and structure in the three studied species. *A. prasinus* and *P. olivaceous* belong to different genera of the subfamily Rutelinae, while *X. eucalypti* belongs to the subfamily Melolonthinae. Yet, all three species have very thin cuticles (here considered synonymous with the upper lamination) between 22 and 57 nm, and the transmittance profile suggests that they contain similar pigment nanoparticles possibly less than 50 nm diameter [11]. The origins of these green cuticles are intriguing. The most common pigments observed in beetles are melanins, ommochromes, carotenoids and flavonoids [75]. In the leaf beetle *Gastrophysa viridula,* it has been proposed that a thin outermost green layer (absorption between 530 and 550 nm) contains quinones and melanin [61]. Another possibility is that the green colour is produced by mixtures of blue tetrapyrroles (bile pigments) and yellow plant-derived carotenoids as in other plant eating insects [75,76]. Further studies are needed to confirm the presence and absorption profile of the pigments in the cuticle of different green scarab species, to determine if their absorption profile varies according to the environment in the chitin matrix, and to evaluate if the pigments of different species have independent evolutionary and/or developmental origins.

Given that this is the first observation of a broadband reflective white underlay in the beetle elytra, we can only hypothesize its biological function. The presence of a pigment-based filter overlying a white NIR reflective structure is an elegant solution to allow reflectance in different wavebands lacking in a single structure. This may be an adaptation to different selective pressures. For example, an untested hypothesis for the broad band scattering produced by some scarabs in the subfamily Melolonthinae [63,65] is that it is useful for camouflage against local white fungi. A non-mutually exclusive hypothesis is that broad band reflection extending to the NIR can aid in passive thermoregulation [9,71,77]. The species studied in this experiment may exploit the versatility of composite materials for passive thermoregulation (maximizing the reflected light and reducing the amount of radiative energy transferred to the beetle body) while maintaining a green appearance favourable for camouflage against a green background, e.g. a forest or any other habitat rich in vegetation. Conversely, some species of insects benefit from a light trapping mechanism to increase their temperature efficiently until they achieve their optimal temperatures [70] and this could be the case for beetle if there is heat transfer between the elytra and body. The air trapped in the densely packed structure such as the one in *A. prasinus* underlay could also favour thermal insulation, but measurements of emissivity of the beetle body and elytra would be needed to support this hypothesis. The absence of air sacs in the elytra of some species may also have specific mechanical functions such as providing extra resistance to fracture or collapse of the elytra [78] or cushioning to reduce the energy transfer to the beetle body and internal organs [79]. However, beetles with larger air sacs are more likely to rely on flight since these adaptations facilitate the demands of aerial locomotion [2]. Furthermore, natural composite materials are invariably

multifunctional and it is possible that more than one selective pressure has driven the evolution of the white underlay in these scarabs. Ecological habits, microhabitat data and behavioural experiments are needed to better understand the biological relevance of the composite structure of the elytra for each species.

Studying natural composite materials and their biological significance has the potential to inform passive cooling technologies. Natural materials combine characteristics that allow them to outperform human-fabricated technologies; they can absorb specific wavelengths in the visible spectrum while still allowing more than 80% NIR reflectance [11]. This is a desirable feature in technologies such as coatings to control the temperature of buildings by minimizing radiative heat transferred to the building while simultaneously achieving the desired colour [11]. In addition, air pockets in a composite material are useful as barrier materials for food packing [80] or to enhance thermal insulation in textiles [81] and even increasing fire resistance in light weight cement to implement in construction [82]. Further research could focus on comparing the effectiveness and scalability of different geometries of the scatterers and the self-assemble properties of natural composite materials.

Credit athor statement

Laura Ospina-Rozo: conceptualization, investigation, formal analysis, visualization and original draft. **Niken Priscilla:** software **James Hutchison:** methodology, investigation and writing-review and editing. **Allison Van de Meene:** methodology, investigation and writing-review and editing. **Nicholas W. Roberts:** conceptualization, writing-review and editing. **Devi Stuart-Fox:** conceptualization, writing-review and editing, supervision. **Ann Roberts:** conceptualization, software, writing-review and editing and supervision.

Funding

This work was supported by funding from the Australian Research Council (grant numbers DP190102203, FT180100216, and FT180100295) and the Australian Research Council Centre of Excellence Scheme (grant numbers CE200100010 and CE170100026), the research grant from the Air Force Office of Scientific Research (AFOSR)/European Office of Aerospace Research and Development (EOARD) (grant number FA9550-19-1-7005) to N.W.R and the University of Melbourne Bioinspiration Hallmark Research Initiative. These funding sources facilitated equipment and talent acquisition but were not involved in the study design, data collection or analysis, manuscript preparation or decision to submit.

Data accessibility

The raw data and processed data required to reproduce these findings are available to download in GitHub (interactive HTML version of the code) and in MendeleyData [83] in the https://doi.org/10.17632/7725svpmy4.1 .

Declaration of competing interest

The authors declare that they have no known competing financial interests or personal relationships that could have appeared to influence the work reported in this paper.

Data availability

I have included a link to the interactive webpage of my code and the raw data in my manuscript. Both data and code were also stored in Mendeley Data Repository. The raw data and processed data required to reproduce these findings are available to download in GitHub (interactive HTML version of the code) and in MendeleyData [83] in the https://doi.org/10.17632/7725svpmy4.1 .

Acknowledgements

We are grateful to the beetle division of the Australian National Insect Collection, especially to Bronte Sinclair, Debbie Jennings and Cate Lemann. We are grateful to Richard O. Prum for kindly sharing his code for the analysis of quasi-coherent scattering by natural photonic structures. Electron microscopy was undertaken in the BioSciences Microscopy Unit, The University of Melbourne.

Appendix A. Supplementary data

Supplementary data to this article can be found online at https://doi.org/10.1016/j.mtadv.2023.100363.

References

[1] T.B.H. Schroeder, J. Houghtaling, B.D. Wilts, M. Mayer, It's not a bug, it's a feature: functional materials in insects, Adv. Mater. 30 (2018), e1705322, https://doi.org/10.1002/adma.201705322.
[2] J. Rivera, S. Murata, M.S. Hosseini, A.A. Trikanad, R. James, A. Pickle, N. Yaraghi, N. Matsumoto, W. Yang, D.Y. Parkinson, H.S. Barnard, P. Zavattieri, A. Arakaki, D. Kisailus, Structural design variations in beetle elytra, Adv. Funct. Mater. 31 (2021), https://doi.org/10.1002/adfm.202106468.
[3] Z. Chen, Z. Zhang, Y. Wang, D. Xu, Y. Zhao, Butterfly inspired functional materials, Mater. Sci. Eng. R Rep. 144 (2021), https://doi.org/10.1016/j.mser.2020.100605.
[4] M. Srinivasarao, Nano-optics in the biological world: beetles, butterflies, birds, and moths, Chem. Rev. 99 (1999) 1935–1961, https://doi.org/10.1021/cr970080y.
[5] M.D. Shawkey, N.I. Morehouse, P. Vukusic, A protean palette: colour materials and mixing in birds and butterflies, J. Royal Soc. Interface 6 (Suppl 2) (2009) S221–S231, https://doi.org/10.1098/rsif.2008.0459.focus.
[6] P. Vukusic, J.R. Sambles, Photonic structures in biology, Nature 424 (2003), https://doi.org/10.1038/nature01941.
[7] J. Teyssier, S.V. Saenko, D. van der Marel, M.C. Milinkovitch, Photonic crystals cause active colour change in chameleons, Nat. Commun. 6 (2015) 6368, https://doi.org/10.1038/ncomms7368.
[8] H. Gonome, M. Nakamura, J. Okajima, S. Maruyama, Artificial chameleon skin that controls spectral radiation: development of Chameleon Cool Coating (C(3)), Sci. Rep. 8 (2018) 1196, https://doi.org/10.1038/s41598-018-19498-5.
[9] D. Stuart-Fox, E. Newton, R.A. Mulder, L. D'Alba, M.D. Shawkey, B. Igic, The microstructure of white feathers predicts their visible and near-infrared reflectance properties, PLoS One 13 (2018), e0199129, https://doi.org/10.1371/journal.pone.0199129.
[10] D. Stuart-Fox, E. Newton, S. Clusella-Trullas, Thermal Consequences of Colour and Near-Infrared Reflectance, vol. 372, Philosophical Transactions of the Royal Society B: Biological Sciences, 2017, https://doi.org/10.1098/rstb.2016.0345.
[11] Y. Chen, J. Mandal, W. Li, A. Smith-Washington, C.-C. Tsai, W. Huang, S. Shrestha, N. Yu, R.P.S. Han, A. Cao, Y. Yang, Colored and paintable bilayer coatings with high solar-infrared reflectance for efficient cooling, Sci. Adv. 6 (2020), https://doi.org/10.1126/sciadv.aaz5413.
[12] J. Mandal, Y. Yang, N. Yu, A.P. Raman, Paints as a scalable and effective radiative cooling technology for buildings, Joule 4 (2020) 1350–1356, https://doi.org/10.1016/j.joule.2020.04.010.
[13] M. Chen, D. Pang, J. Mandal, X. Chen, H. Yan, Y. He, N. Yu, Y. Yang, Designing mesoporous photonic structures for high-performance passive daytime radiative cooling, Nano Lett. 21 (2021) 1412–1418, https://doi.org/10.1021/acs.nanolett.0c04241.
[14] J. Mandal, Y. Fu, A. Overvig, M. Jia, K. Sun, N. Shi, H. Zhou, X. Xiao, N. Yu, Y. Yang, Hierarchically porous polymer coatings for highly efficient passive daytime radiative cooling, Science 362 (2018) 315–319, https://doi.org/10.1126/science.aat9513.
[15] A. Rosati, M. Fedel, S. Rossi, NIR reflective pigments for cool roof applications: a comprehensive review, J. Clean. Prod. 313 (2021), https://doi.org/10.1016/j.jclepro.2021.127826.
[16] J.d.O. Primo, K.W. Borth, D.C. Peron, V.d.C. Teixeira, D. Galante, C. Bittencourt, F.J. Anaissi, Synthesis of green cool pigments (CoxZn1-xO) for application in NIR radiation reflectance, J. Alloys Compd. 780 (2019) 17–24, https://doi.org/10.1016/j.jallcom.2018.11.358.
[17] N.E. Stork, How many species of insects and other terrestrial arthropods are there on earth? Annu. Rev. Entomol. 63 (2018) 31–45, https://doi.org/10.1146/annurev-ento-020117-043348.

[18] J.F. Lawrence, A.F. Newton, Evolution and clasification of beetles, Annu. Rev. Ecol. Systemat. 13 (1982) 261–290. https://www.jstor.org/stable/2097069.
[19] A.C. Neville, Biology of the Arthropod Cuticle, Springer-Verlag Berlin and Heidelberg GmbH & Co. KG, Berlin, Germany, 2011.
[20] T. Van de Kamp, G. Hartmut, On the architecture of beetle elytra, Entomologie heute 22 (2010) 191–204.
[21] C. He, Q. Zu, J. Chen, M.N. Noori, A review of the mechanical properties of beetle elytra and development of the biomimetic honeycomb plates, J. Sandw. Struct. Mater. 17 (2015) 399–416, https://doi.org/10.1177/1099636215576881.
[22] J. Chen, X. Zhang, Y. Okabe, J. Xie, M. Xu, Beetle elytron plate and the synergistic mechanism of a trabecular-honeycomb core structure, Sci. China Technol. Sci. 62 (2018) 87–93, https://doi.org/10.1007/s11431-018-9290-1.
[23] A.E. Seago, P. Brady, J.P. Vigneron, T.D. Schultz, Gold bugs and beyond: a review of iridescence and structural colour mechanisms in beetles (Coleoptera), J. Royal Soc. Interface 6 (Suppl 2) (2009) S165–S184, https://doi.org/10.1098/rsif.2008.0354.focus.
[24] J. Lomakin, P.A. Huber, C. Eichler, Y. Arakane, K.J. Kramer, R.W. Beeman, M.R. Kanost, S.H. Gehrke, Mechanical properties of the beetle elytron, a biological composite material, Biomacromolecules 12 (2011) 321–335, https://doi.org/10.1021/bm1009156.
[25] M. Iwamoto, J. Ched, K. Kurashiki, Q.-Q. Ni, Chitin fibre and its laminated structure of the fore-wing of beetle, High Perform. Struct. Composites 59 (2002).
[26] E.D. Finlayson, L.T. McDonald, P. Vukusic, Optically ambidextrous circularly polarized reflection from the chiral cuticle of the scarab beetle Chrysina resplendens, J. Royal Soc. Interface 14 (2017), https://doi.org/10.1098/rsif.2017.0129.
[27] V. Sharma, M. Crne, J.O. Park, M. Srinivasarao, Bouligand structures underlie circularly polarized iridescence of scarab beetles: a closer view, Mater. Today Proc. 1 (2014) 161–171, https://doi.org/10.1016/j.matpr.2014.09.019.
[28] H. Arwin, R. Magnusson, J. Landin, K. Järrendahl, Chirality-induced polarization effects in the cuticle of scarab beetles: 100 years after Michelson, Phil. Mag. 92 (2012) 1583–1599, https://doi.org/10.1080/14786435.2011.648228.
[29] A. Zaheri, J.S. Fenner, B.P. Russell, D. Restrepo, M. Daly, D. Wang, C. Hayashi, M.A. Meyers, P.D. Zavattieri, H.D. Espinosa, Revealing the mechanics of helicoidal composites through additive manufacturing and beetle developmental stage analysis, Adv. Funct. Mater. 28 (2018), https://doi.org/10.1002/adfm.201803073.
[30] M. Mitov, Cholesteric liquid crystals in living matter, Soft Matter 13 (2017) 4176–4209, https://doi.org/10.1039/C7SM00384F.
[31] L. Wang, A.M. Urbas, Q. Li, Nature-Inspired emerging chiral liquid crystal nanostructures: from molecular self-assembly to DNA mesophase and nanocolloids, Adv. Mater. 32 (2020), e1801335, https://doi.org/10.1002/adma.201801335.
[32] C. Boyon, V. Soldan, M. Mitov, Bioinspired, cholesteric liquid-crystal reflectors with time-controlled coexisting chiral and achiral structures, ACS Appl. Mater. Interfaces 13 (2021) 30118–30126, https://doi.org/10.1021/acsami.1c08218.
[33] J.D. Pye, The distribution of circularly polarized light reflection in the Scarabaeoidea (Coleoptera), Biol. J. Linn. Soc. 100 (2010) 585–596, https://doi.org/10.1111/j.1095-8312.2010.01449.x.
[34] L. Ospina-Rozo, A. Roberts, D. Stuart-Fox, A generalized approach to characterise optical properties of natural objects, Biol. J. Linn. Soc. (2022). In Press.
[35] R.O. Prum, R.H. Torres, S. Williamson, J. Dyck, Two-dimensional Fourier analysis of the spongy medullary keratin of structurally coloured feather barbs, Proceedings Royal Soc. 266 (1999), https://doi.org/10.1098/rspb.1999.0598.
[36] R.O. Prum, R.H. Torres, A Fourier tool for the analysis of coherent light scattering by bio-optical nanostructures, Integr. Comp. Biol. 43 (2003) 591–602, https://doi.org/10.1093/icb/43.4.591.
[37] S.R. Mouchet, S. Luke, L.T. McDonald, P. Vukusic, Optical costs and benefits of disorder in biological photonic crystals, Faraday Discuss 223 (2020) 9–48. https://www.ncbi.nlm.nih.gov/pubmed/33000817.
[38] S. Johnsen, The Optics of Life: A Biologist's Guide to Light in Nature, Princeton University Press, 2012.
[39] L. Ospina-Rozo, A. Roberts, D. Stuart-Fox, A generalized approach to characterise optical properties of natural objects Biological, J. Linnean Soc. 10 (2022) 1–22.
[40] R. Maia, H. Gruson, J.A. Endler, T.E. White, B. R, O'Hara, pavo 2: new tools for the spectral and spatial analysis of colour in r, Methods Ecol. Evol. 10 (2019) 1097–1107, https://doi.org/10.1111/2041-210X.13174.
[41] J. Schindelin, I. Arganda-Carreras, E. Frise, V. Kaynig, M. Longair, T. Pietzsch, S. Preibisch, C. Rueden, S. Saalfeld, B. Schmid, J.Y. Tinevez, D.J. White, V. Hartenstein, K. Eliceiri, P. Tomancak, A. Cardona, Fiji: an open-source platform for biological-image analysis, Nat. Methods 9 (2012) 676–682, https://doi.org/10.1038/nmeth.2019.
[42] P. Vukusic, D.G. Stavenga, Physical methods for investigating structural colours in biological systems, J. R. Soc. Interface 6 (Suppl 2) (2009) S133–S148, https://doi.org/10.1098/rsif.2008.0386.focus.
[43] T.J. Deerinck, E.A. Bushong, V. Lev-Ram, X. Shu, R.Y. Tsien, M.H. Ellisman, Enhancing serial block-face scanning electron microscopy to enable high resolution 3-D nanohistology of cells and tissues, Microsc. Microanal. 16 (2010) 1138–1139, https://doi.org/10.1017/S1431927610055170.
[44] S. Lippens, A. Kremer, P. Borghgraef, C.J. Guerin, Serial block face-scanning electron microscopy for volume electron microscopy, Methods Cell Biol. 152 (2019) 69–85, https://doi.org/10.1016/bs.mcb.2019.04.002.
[45] R. R Core Team, R, A Language and Environment for Statistical Computing, R Foundation for Statistical Computing, Vienna - Austria, 2021.
[46] J.R. Kremer, D.N. Mastronarde, R. McIntosh, Computer visualization of three-dimensional image data using IMOD, J. Struct. Biol. 116 (1996) 71–76. https://bio3d.colorado.edu/imod/.
[47] COMSOL Multiphysics®, in: C. AB (Ed.), Stockholm - Sweden.
[48] H.L. Leertouwer, B.D. Wilts, D.G. Stavenga, Refractive Index and Dispersion of Butterfly Chitin and Bird Keratin Measured by Polarizing Interference Microscopy, vol. 19, 2011.
[49] D.E. Azofeifa, H.J. Arguedas, W.E. Vargas, Optical properties of chitin and chitosan biopolymers with application to structural color analysis, Opt. Mater. 35 (2012) 175–183.
[50] J. Lafaita, C. Andrauda, S. Berthiera, J. Boulengueza, P. Calletb, S. Dumazetb, M. Rassartc, J.-P. Vigneronc, Modeling the vivid white color of the beetle Calothyrza margaritifera, Mater. Sci. Eng. B (2010) 169.
[51] S.M. Luke, B.T. Hallam, P. Vukusic, Structural optimization for broadband scattering in several ultra-thin white beetle scales, Appl. Opt. 49 (2010) 4246–4254, https://doi.org/10.1364/ao.49.004246.
[52] B.T. Hallam, A.G. Hiorns, P. Vukusic, Developing optical efficiency through optimized coating structure: biomimetic inspiration from white beetles, Appl. Opt. 48 (2009) 3243–3249, https://doi.org/10.1364/AO.48.003243.
[53] S.H. Lee, S.M. Han, S.E. Han, Anisotropic diffusion in Cyphochilus white beetle scales, APL Photonics 5 (2020), https://doi.org/10.1063/1.5144688.
[54] M. Sun, A. Liang, G.S. Watson, J.A. Watson, Y. Zheng, L. Jiang, Compound microstructures and wax layer of beetle elytral surfaces and their influence on wetting properties, PLoS One 7 (2012), https://doi.org/10.1371/journal.-pone.0046710 e46710.
[55] D. Zhao, H. Yang, Z. Ma, W. Zhou, Polarization independent broadband reflectors based on cross-stacked gratings, Opt Express 19 (2011).
[56] J.F. Harrison, Tracheal System, Encyclopedia of Insects, Elsevier, 2009, pp. 1011–1015.
[57] V.B. Wigglesworth, The properties of the lining membrane of the insect tracheal system, Tissue Cell (1990) 22.
[58] V.B. Meyer-Rochow, G.A. Horridge, The Eye of Anoplognathus (Coleoptera, Scarabeidae), Proceedings of the Royal Society of London B, 1975, p. 188.
[59] M. Dacke, P. Nordström, C.H. Scholtz, Twilight orientation to polarised light in the crepuscular dung beetle Scarabaeus zambesianus, J. Exp. Biol. 206 (2003) 1535–1543.
[60] N. Gokan, The compound eye of the soybean beetle, Anomala rufocuprea Motschulsky (Coleoptera: scarabaeidae), Appl. Entomol. Zool 17 (1982) 227–237.
[61] O.D. Onelli, T.V. Kamp, J.N. Skepper, J. Powell, T.D.S. Rolo, T. Baumbach, S. Vignolini, Development of structural colour in leaf beetles, Sci. Rep. 7 (2017) 1373, https://doi.org/10.1038/s41598-017-01496-8.
[62] V.E. Johansen, O.D. Onelli, L.M. Steiner, S. Vignolini, Photonics in nature: from order to disorder, in: S. Gorb, E. Gorb (Eds.), Functional Surfaces in Biology III., Springer International Publishing, Cham, Switzerland, 2017, pp. 53–89.
[63] B.D. Wilts, X. Sheng, M. Holler, A. Diaz, M. Guizar-Sicairos, J. Raabe, R. Hoppe, S.H. Liu, R. Langford, O.D. Onelli, D. Chen, S. Torquato, U. Steiner, C.G. Schroer, S. Vignolini, A. Sepe, Evolutionary-Optimized photonic network structure in white beetle wing scales, Adv. Mater. 30 (2018), e1702057, https://doi.org/10.1002/adma.201702057.
[64] S.L. Burg, A.L. Washington, J. Villanova, A.J.C. Dennison, D. McLoughlin, O.O. Mykhaylyk, P. Vukusic, W. Furnass, R.A.L. Jones, A.J. Parnell, J.P.A. Fairclough, X-ray nano-tomography of complete scales from the ultra-white beetles Lepidiota stigma and Cyphochilus, Sci. Data 7 (2020) 163, https://doi.org/10.1038/s41597-020-0502-y.
[65] M. Burresi, L. Cortese, L. Pattelli, M. Kolle, P. Vukusic, D.S. Wiersma, U. Steiner, S. Vignolini, Bright-white beetle scales optimise multiple scattering of light, Sci. Rep. 4 (2014) 6075, https://doi.org/10.1038/srep06075.
[66] M.R. Slaton, E. Raymond Hunt, W.K. Smith, Estimating near-infrared leaf reflectance from leaf structural characteristics, Am. J. Bot. 88 (2001) 278–284, https://doi.org/10.2307/2657019.
[67] H.W. Gausman, W.A. Allen, R. Cardenas, Reflectance of cotton leaves and their structure 1, Rem. Sens. Environ. (1999) 1.
[68] D.E. McCoy, T. Feo, T.A. Harvey, R.O. Prum, Structural absorption by barbule microstructures of super black bird of paradise feathers, Nat. Commun. 9 (2018) 1. https://www.ncbi.nlm.nih.gov/pubmed/29317637.
[69] D.E. McCoy, R.O. Prum, Convergent evolution of super black plumage near bright color in 15 bird families, J. Exp. Biol. 222 (2019). https://www.ncbi.nlm.nih.gov/pubmed/31558610.
[70] K. Shanks, S. Senthilarasu, R.H. Ffrench-Constant, T.K. Mallick, White butterflies as solar photovoltaic concentrators, Sci. Rep. 5 (2015), 12267. https://www.ncbi.nlm.nih.gov/pubmed/26227341.
[71] W. Zhang, X. Zhao, Y. Xiong, W. Wang, D. Zhang, Achieve Structural White Inspired from Quasiordered Microstructures in Morpho Theseus, 2022.
[72] T.M. Jordan, J.C. Partridge, N.W. Roberts, Disordered animal multilayer reflectors and the localization of light, J. R. Soc. Interface 11 (2014), 20140948. https://www.ncbi.nlm.nih.gov/pubmed/25339688.
[73] D. Gur, B.A. Palmer, S. Weiner, L. Addadi, Light manipulation by guanine crystals in organisms: biogenic scatterers, mirrors, multilayer reflectors and photonic crystals, Adv. Funct. Mater. 27 (2017).
[74] S. Magkiriadou, J.G. Park, Y.S. Kim, V.N. Manoharan, Absence of red structural color in photonic glasses, bird feathers, and certain beetles, Phys. Rev. E: Stat.,

Nonlinear, Soft Matter Phys. 90 (2014), 062302, https://doi.org/10.1103/physreve.90.062302.
[75] R. Futahashi, M. Osanai-Futahashi, Pigments in Insects, Pigments, Pigment Cells and Pigment Patterns, 2021, pp. 3–43.
[76] G. Shamim, S.K. Ranjan, D.M. Pandey, R. Ramani, Biochemistry and biosynthesis of insect pigments, Eur. J. Entomol. 111 (2014) 149–164.
[77] D. Xie, Z. Yang, X. Liu, S. Cui, H. Zhou, T. Fan, Broadband omnidirectional light reflection and radiative heat dissipation in white beetles Goliathus goliatus, Soft Matter 15 (2019) 4294–4300, https://doi.org/10.1039/c9sm00566h.
[78] J. Chen, N. Hao, L. Pan, L. Hu, S. Du, Y. Fu, Characteristics of compressive mechanical properties and strengthening mechanism of 3D-printed grid beetle elytron plates, J. Mater. Sci. 55 (2020) 8541–8552.
[79] L. Kundanati, S. Signetti, H.S. Gupta, M. Menegon, N.M. Pugno, Multilayer stag beetle elytra perform better under external loading via non-symmetric bending properties, J. R. Soc. Interface 15 (2018). https://www.ncbi.nlm.nih.gov/pubmed/30045895.
[80] Z. Yu, Y. Ji, V. Bourg, M. Bilgen, J.C. Meredith, Chitin- and cellulose-based sustainable barrier materials: a review, Emergent Mater. 3 (2020) 919–936.
[81] J. Sun, F. Cai, D. Tao, Q. Ni, Y. Fu, Enhanced thermal insulation of the hollow glass microsphere/glass fiber fabric textile composite material, Polymers 13 (2021), https://doi.org/10.3390/polym13040505.
[82] S.K. Adhikary, D.K. Ashish, Ž. Rudžionis, Aerogel based thermal insulating cementitious composites: a review, Energy Build. 245 (2021), https://doi.org/10.1016/j.enbuild.2021.111058.
[83] L. Ospina-Rozo, N. Priscilla, J. Hutchison, A. Van de Meene, N. Roberts, D. Stuart-Fox, A. Roberts, Deconstructed Beetles: Green Composite Materials with Potential for Passive Cooling Due to High Near-Infrared Reflectivity - Data and Code, Mendeley Data, 2022.